Filament Crimp in Three Dimensions Measured by Image Analysis and Fractal Geometry

TAE JIN KANG AND JAE YEOL LEE

Department of Fiber and Polymer Science, Seoul National University, Seoul, South Korea

ABSTRACT

Image analysis and fractal geometry are used to define the three dimensional structure of filament crimping. The images are formed using a single charge coupled device (CCD) camera and a single mirror. Placed near the filament and at 45 degrees to the viewing direction, the mirror allows the camera to collect two orthogonal views of the sample, which are combined to give the *xyz* coordinates of every point on the filament. The crimp ratio and fractal dimension can then easily be calculated from these data. Recasting the data in cylindrical polar coordinates immediately shows details of the crimp property, such as the size and planarity of the crimped structure.

Most natural fibers have curled structures. Since the curled wave causes a soft, rich feeling, it is an important factor that provides aesthetic and sensuous values to textile products. For synthetic fibers, a texturing process is necessary to provide a luxurious and natural impressions. However, it is not easy to assess crimp in fibers because of its delicate structure.

In an earlier work (Kang *et al.* [3]), we proposed fractal geometry as a quantitative method to deal with the planar image of the complex crimp structure. In this study, we devise a new optical method to capture the three-dimensional shape of the filament crimp more exactly and easily, and we apply the fractal dimension in addition to other geometric parameters.

Trials for the 3D Measurement

Various methods to measure the 3D structure of an object have been tried. A probe is the simplest method, which reads the surface height by direct contact with an object. However, it cannot be used for tender textile materials. The laser detector is used to detect the distance to an object with high-powered resolution, but it is not proper for textiles because of its excessive sensitivity to hairs or chemicals on the fibers. 3D scanner equipment is costly and still under development. Recently, diverse optical measurements have emerged as the result of quick advances in computer vision technology. The scanning moiré method [2, 4], the line profile image [5], and the stereo camera system [1] are frequently used. The scanning moiré method uses a grating projector and a scanning device. The grating projector makes many light or dark stripes on the projected surface, called moiré fringe patterns. The scanning device captures these moiré fringe patterns and provides information about the height of the surface. The line profile image method uses a line projector. When the line beam is incident upon an object, the line is deformed on the surface by its prominence and depression. The surface shape can then be reconstructed using a combination of these deformed profile images at various positions. The stereo camera system works as human eyes do. Two cameras take different images of one object from different viewing angles. After calibrating the two images, matching the identical points, and detecting the disparity in them, one can obtain 3D information on an object.

We have developed a new method to obtain 3D data on crimped filaments. It is based on the idea of the stereo camera system, but uses a single camera assisted by a mirror.

3D Capture of Filament Crimp

In 3D capture of filament crimping, it is not possible to use probes, laser detectors, moiré fringe patterns, or profile images because of the filament's single skeleton. The stereo camera system may therefore be a candidate, but the image matching process between the stereo images is notorious for difficulties in recognizing identical points. Furthermore, inevitable inequalities decrease the reliance of the matching process: for example the inequality of signal reception between two cameras, the different optical properties of a lens, and the inaccuracy of distance and angle between the two cameras. Correcting for different brightness values and aligning images with tilt or rotation require considerable effort. In this work, these problems are avoided.

Figure 1 shows the experimental configuration. If the camera captures the image of filament crimp without a mirror, as in Figure 1a, the captured image is an orthogonal projection on the XY plane of the crimp. The camera installed with the mirror, as in Figure 1b, can capture the images of the orthogonal projections not only on the XY plane (front view) but also on the XZ plane (side view). This method provides 3D information about the position of every point of the filament without troublesome matching algorithms. Figure 2 explains the relation between the world coordinate (X, Y, Z) and the image coordinates (x, y), (x, y'). Figure 2a is the lateral view of focusing. Every point on the filament is converted from the world coordinate X to the image coordinate x. Figure 2b shows the focusing viewed from above. The direct image of the filament is focused on the image plane as a point (x, y), while the mirror image is a point (x, y'). The split images have same images coordinate x because their world coordinate X is the same, but they have different image coordinates y and y' because the mirror image is shifted in the Y direction.

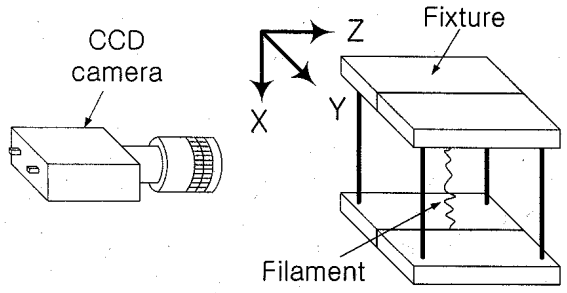

(a) Setup without mirror

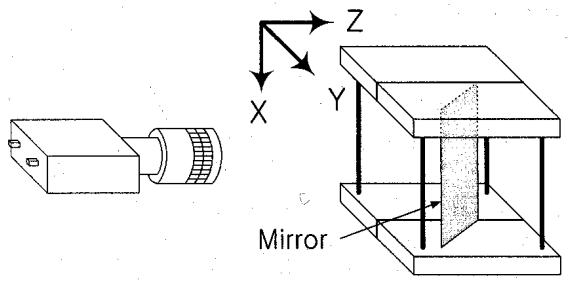

(b) Setup with mirror

FIGURE 1. Configuration for the 3D capture of crimp wave with a single CCD camera and a single mirror.

The relation between the world coordinate (X, Y, Z) and the image coordinates (x, y), (x, y') can be summarized in the following form:

$$\begin{pmatrix} X \\ Y \\ Z \end{pmatrix} = \mathbf{M}\begin{pmatrix} x \\ y \\ y' \end{pmatrix} + \mathbf{T} \quad . \tag{1}$$

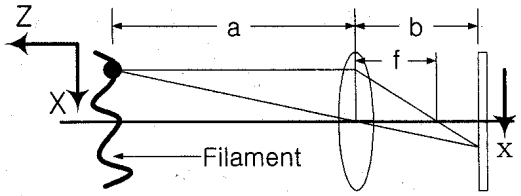

(a) Lateral view of focusing

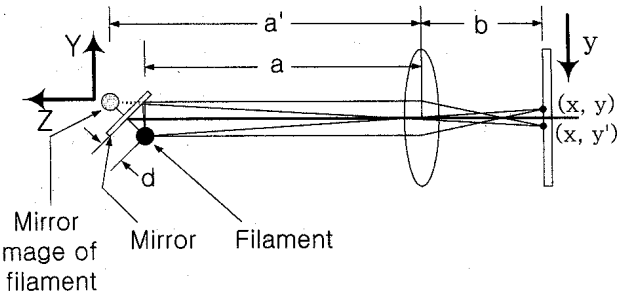

(b) Planar view of focusing

FIGURE 2. Relation between world coordinate and image coordinate.

The tensors **M**, **T** are transformations of magnification and translation, respectively. The images do not have rotation and tilt in this right-shot configuration. The following equations are derived from the lens formula:

$$(X - t_1) : (-x - t_2) = a : b$$

$$bX = -ax + bt_1 - at_2$$

$$\therefore X = -\frac{a}{b}x + T_1 \quad , \tag{2}$$

$$(Y - t_3) : (y - t_4) = a : b$$

$$bY = ay + bt_3 - at_4$$

$$\therefore Y = \frac{a}{b}x + T_2 \quad , \tag{3}$$

$$(Z - t_5) : (-y' - t_6) = a' : b$$

$$bZ = -a'y' + bt_5 - a't_6$$

$$\therefore Z = -\frac{a'}{b}x + T_3 \quad . \tag{4}$$

The values from t_1 to t_6 mean the displacement from the origin. So T_1, T_2, T_3 are constants dependent on the experimental settings. Now, Equation 1 is complemented by Equations 2, 3, and 4:

$$\begin{pmatrix} X \\ Y \\ Z \end{pmatrix} = \begin{pmatrix} -\frac{1}{m} & 0 & 0 \\ 0 & \frac{1}{m} & 0 \\ 0 & 0 & -\frac{1}{m'} \end{pmatrix} \begin{pmatrix} x \\ y \\ y' \end{pmatrix} + \begin{pmatrix} T_1 \\ T_2 \\ T_3 \end{pmatrix} , \quad (5)$$

where $m\left(=\frac{b}{a}\right)$, $m'\left(=\frac{b}{a'}\right)$ are the magnification of the lens. In the experiment, the mirror is placed almost on the filament to allow the direct image and the mirror image to be focalized in one frame at a time within the depth of focus. This means that the value of d decreases ($d \to 0$), resulting in $a \approx a'$ and $m \approx m'$.

Fractal Dimension of Filament Crimp

PET filament yarns (75d/36f) were textured on nip belt texturing machines at different twist levels to change their crimp levels. The belt cross angle varied from 90° to 130°, with other texturing conditions fixed. Sample images were obtained with the color CCD camera, whose output was an NTSC format with 682(H) × 492(V) pixels.

After calculating the 3D world coordinate for every point in the filament crimp, we reconstructed the shape of the crimp wave in the computer memory and applied fractal geometry to evaluate its complexity. The fractal dimension D is taken from the slope of linear regression in the double logarithm plot between the scale factor of box size s and the number of occupied boxes $N(s)$ as in following equation from our prior work [3]:

$$\ln N(s) = -D \ln s + C \quad . \quad (6)$$

In this work, we used a 3D cube instead of a 2D square as a covering unit, because the crimp wave is a three-dimensional object. Figure 3 shows this cube counting procedure schematically.

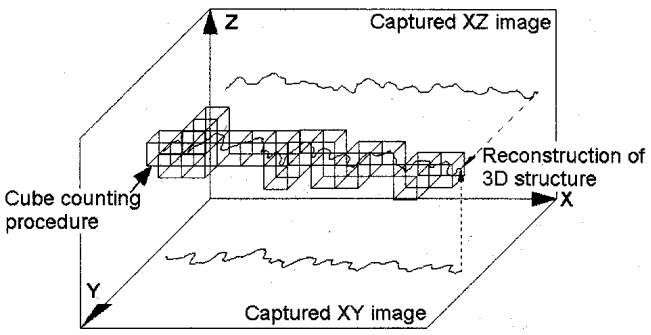

FIGURE 3. Cube counting procedure for the crimp wave.

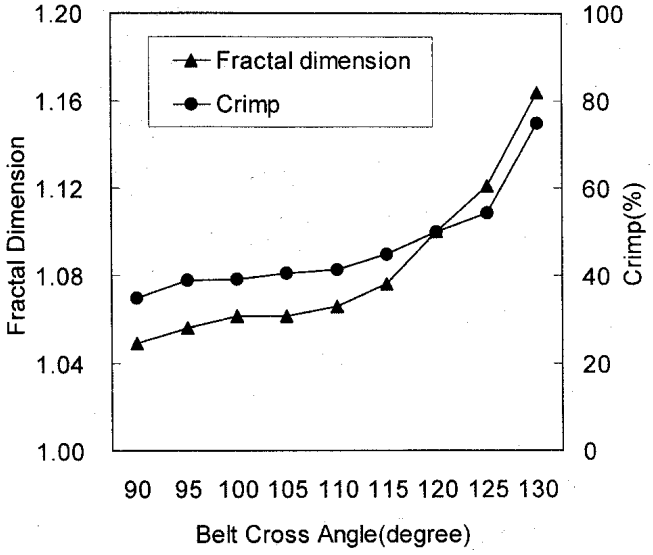

FIGURE 4. Fractal dimension and crimp ratio of filament yarn textured at different belt cross angles.

We also calculated the conventional crimp ratio using the 3D crimp data. The definition of a crimp ratio is the ratio of the increase in the length by unfolding the crimp wave to the initial length before unfolding:

$$\text{Crimp ratio} = \frac{L - L'}{L'} \times 100(\%) \quad . \quad (7)$$

The length before unfolding the crimp L' is equal to the direct length between both ends of the crimp wave, and the length after unfolding the crimp L is equal to its meandering length. This method has objectivity without

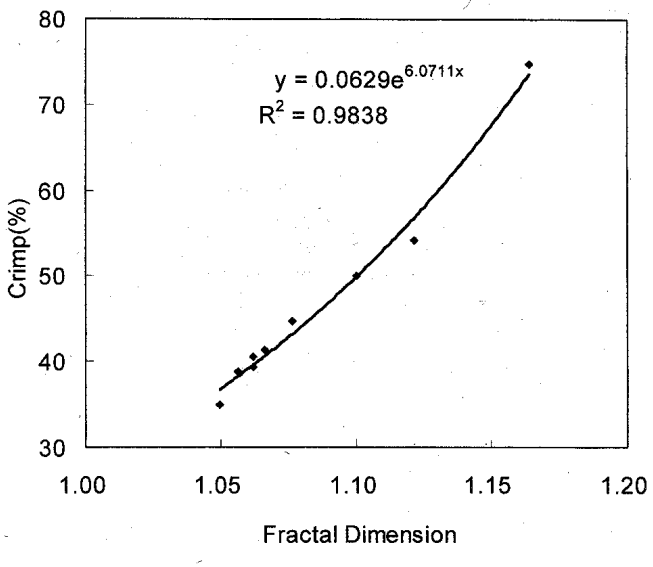

FIGURE 5. Exponential relationship between fractal dimension and crimp ratio.

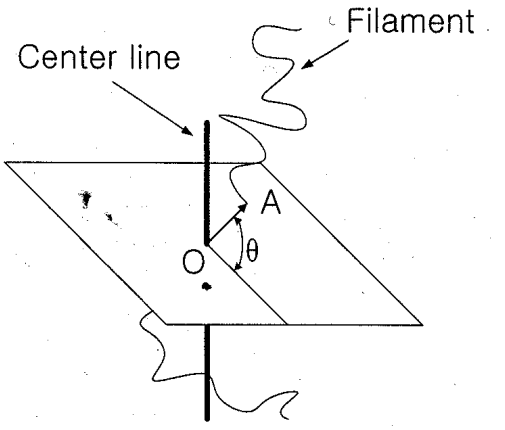

FIGURE 6. Parameters for the crimp property ($\overline{OA}$ = distance from the center line, θ = azimuth angle).

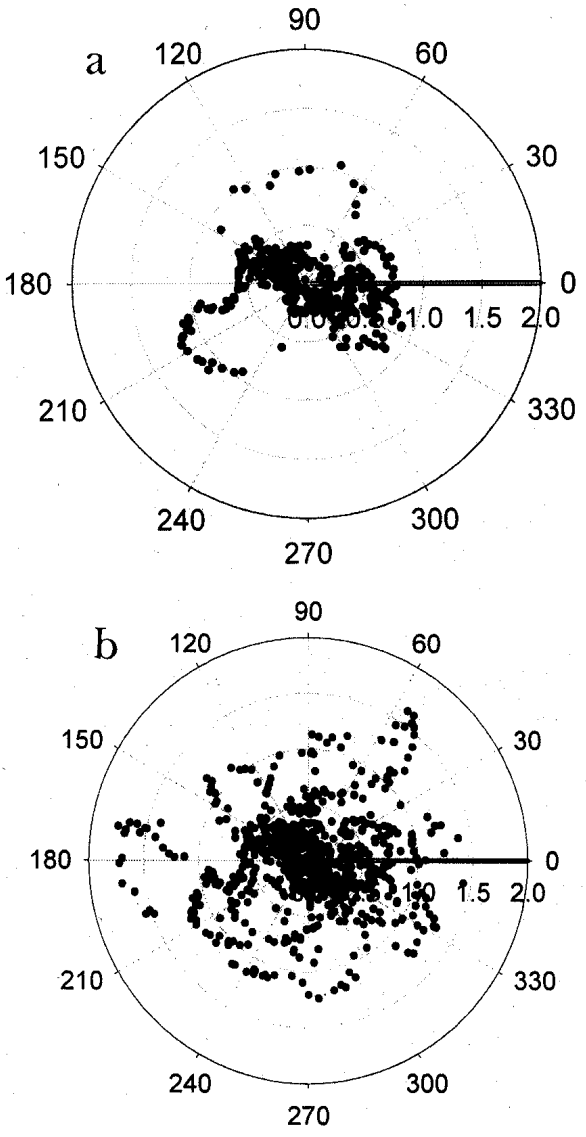

FIGURE 7. Polar coordinate graph between distance and azimuth angle: (a) crimped filament by nip belt cross angle of 90°: (b) crimped filament by nip belt cross angle of 130°.

obscurity when unfolding by hand, preciseness without deformation with direct contact, and easiness and rapidity without tedious work.

Figure 4 shows the results of the fractal dimensions and crimp ratios for the samples. The filaments textured by the large belt cross angle have high values in the fractal dimension and crimp ratio. The fractal dimension is the geometric quantitative value that defines a straight line as 1, a plane as 2, and an intermediate crooked line as the value between 1 and 2 according to its plane-filling property. Filaments with higher values of the fractal dimension therefore have more wandering shapes. In the prior work [3], we revealed that the crimp ratio has an exponential relationship with the fractal dimension, and the result corresponds with the fact that the exponential regression curve fits the experimental data better than any other kind of regression. Figure 5 shows the fitting of the exponential curve.

Characterizing the Crimp Property

The crimp property is as important as the degree of crimp. It is well known that the yarns textured by nip belt texturing, friction disc texturing, pin texturing, and air texturing have a different handle, bulkiness, softness, and resilience due to their different crimp properties.

We characterize the crimp property by its size and planarity. Crimp size can be assessed by the fluctuation of the crimp position from the center line, and the planarity can be assessed by the azimuth angle of the crimp wave. Figure 6 is a schematic diagram of the crimp property. A voluminous crimp wave shows large fluctu-

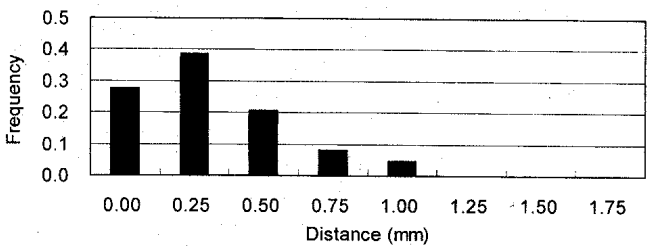

(a) Crimped filament by the nip belt cross angle of 90°

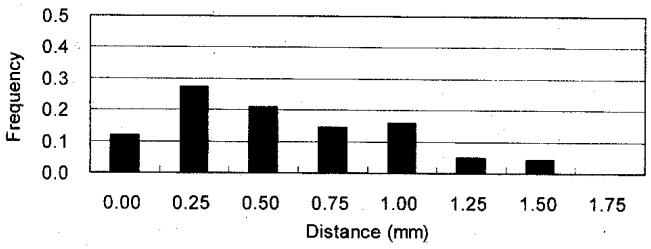

(b) Crimped filament by the nip belt cross angle of 130°

FIGURE 8. Distribution of the distance from the center line.

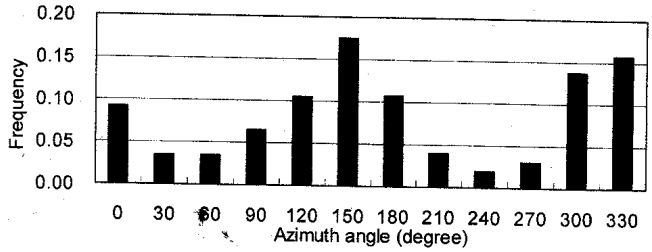

(a) Crimped filament by the nip belt cross angle of 90°

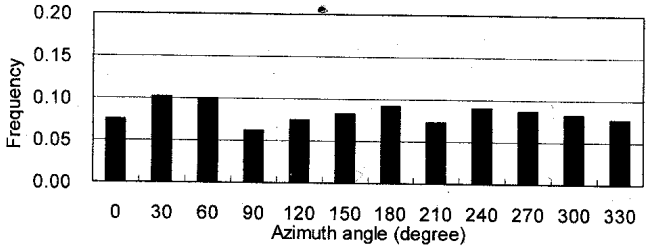

(b) Crimped filament by the nip belt cross angle of 130°

FIGURE 9. Distribution of the azimuth angle.

ations in the length of OA, while the straight filament has a very short length of OA. The distribution of the azimuth angle θ reveals the planarity of the crimp. An azimuth angle distributed impartially represents a lively crimped structure, and an azimuth angle distributed partially represents a flattened structure.

Using the 3D data of the crimp wave, we can easily obtain the distance from the center line and the azimuth angle at every point on the crimp wave. Figure 7 is the polar coordinate graph between the distance and the azimuth angle. Figure 7a shows that most of the crimp wave is within 1 mm, and the azimuth angle is concentrated in some directions. On the other hand, Figure 7b shows a wider reach in the distance and an impartial azimuth angle. Figures 8 and 9 reveal the differences in crimp properties more quantitatively. In Figure 8, the crimp by the nip belt cross angle of 90° shows a lower level of the distance with the average of 0.25, which we define as the average crimp radius (ACR) to assess the size of the crimp wave. The crimp by the nip belt cross angle of 130° shows a higher level of the distance with an ACR of 0.63, which means a more voluminous crimp. In Figure 9, the distribution of the azimuth angle creates more vivid divergence. The crimp by the nip belt cross angle of 90° has a flattened shape in the directions of 150° and 330°, while the other sample has an isotropic shape. We define the planarity factor (PF) as

$$\text{PF} = \frac{\text{the maximum frequency in the azimuth angle}}{\text{the minimum frequency in the azimuth angle}}$$

The PF of Figure 9a is 7.4, while that of Figure 9b is 1.5.

Conclusions

We have developed a new optical noncontact method to obtain 3D data on filament crimp. This method provides a practical and precise way for 3D measurements of crimp waves. The complexity of crimping can be evaluated quantitatively by the fractal dimension, and the crimp property can be characterized by the average crimp radius and the planarity factor.

Literature Cited

1. Helm, J. D., McNeill, S. R., and Sutton, M. A., Improved Three-dimensional Image Correlation for Surface Displacement Measurement, *Optic. Eng.* **35**(7), 1911–1920 (1996).
2. Idesawa, M., Yatagai, T., and Soma, T., Scanning Moiré Method and Automatic Measurement of 3-D Shapes, *Appl. Optics* **16**(8), 2152–2162 (1977).
3. Kang, T. J., Lee, J. Y., Chung, K., and Lee, S. G., Evaluating Yarn Crimp with Fractal Geometry, *Textile Res. J.* **69**(7), 527–534 (1999).
4. Read, D. T., Dally, J. W., and Szanto, M., Scanning Moiré at High Magnification Using Optical Methods, *Exper. Mechan.* **33**, 110–116 (1993).
5. Tai, W., and Changi, M., Noncontact Profilometric Measurement of Large-form Parts, *Optic. Eng.* **35**(9), 2730–2735 (1996).

Manuscript received September 20, 1999; accepted February 2, 2000.